# Equilibrium Theory Analysis of Thermal Regeneration of a Humid Adsorption Column: Selection of Optimal Hot Purge Gas Temperature

# Equilibrium Theory Analysis of Thermal Regeneration of a Humid Adsorption Column: Selection of Optimal Hot Purge Gas Temperature

Hyungwoong Ahn*

*School of Engineering, Institute for Materials and Processes,*

*The University of Edinburgh, Robert Stevenson Road, Edinburgh EH9 3FB, UK*

*Corresponding author. Tel.: +44 131 650 5891

*E-mail address:* H.Ahn@ed.ac.uk

**Abstract**

A Thermal Swing Adsorption (TSA) process has been widely commercialised for its application to air drying. In designing an air-drying TSA, zeolite 13X is chosen as a desiccant when required to produce a very low dew point dry air due to its highly nonlinear, favourable isotherm. It is essential to make use of an external hot purge gas in producing such an extremely low dew point dry air, as the column has to be regenerated thoroughly for the next adsorption step. In case of the externally heated TSA, usage of a hot purge gas gives rise to huge energy consumption. Also the cycle time has to be made as short as possible to enhance the bed productivity. To optimise this energy-intensive process, it is crucial to find an optimal hot purge gas temperature at which the column can be regenerated as quickly as possible with less energy

consumed. In this study, Equilibrium Theory approach was taken to analyse the thermal regeneration breakthrough of a zeolite 13X column saturated with a water vapour in which the equilibrium isotherm is estimated by Toth or Aranovich-Donohue isotherms. As a result of Equilibrium Theory analysis, it was found that the trailing front of a thermal regeneration breakthrough would exhibit a transition of the shape from simple wave to shock wave with increasing purge gas temperature. The purge gas temperature has to be chosen so that after thermal regeneration the targeted water vapour concentration remaining in the column lies within the concentration range occupied by the shock wave. A useful correlation that relates the targeted dew point of the remaining water vapour with the purge gas temperature was proposed. The presence of the optimal hot purge gas temperature estimated by Equilibrium Theory was validated by both full numerical simulation and ideal work consumption.

Keywords: Air-drying; Water; Zeolite 13X; Equilibrium Theory; Thermal Regeneration; Adsorption

## 1. Introduction

An adsorptive drying process has long been employed for drying of gases or liquids [1-5], as it can occupy small footprint and operate continuously thanks to the regenerative nature of a desiccant owning a large drying capacity. A dry air produced by adsorptive drying has been widely used in food and pharmaceutical industries as well as gas processing industry [6-8]. The quality of a dry air is categorised into class 0 to 9 by its contents of solid particles, water and oil, according to ISO 8573-1. For its application to food and pharmaceutical industries, the dry air has to be of excellent quality containing

extremely low water vapour, such as at least less than -40°C dew point (class 2) but more often less than -70°C dew point (class 1) [9].

A variety of cyclic adsorption processes have been devised for air drying so far, being categorised into pressure-swing heatless dryers, temperature-swing dryers with the columns heated internally, temperature-swing dryers with the column regenerated by hot dry or wet air, etc [10-16]. Among them, it is known that a Thermal Swing Adsorption (TSA) process with the column regenerated externally by a hot dry air is capable of producing a dry air at extremely low dew points, often below -70 °C. This is because regenerating the column with a hot dry air ensures the adsorption column being regenerated very rigorously, enabling to produce a very low dew point air in the next adsorption run [3, 4, 10].

Various adsorbents can be chosen as desiccant for an adsorptive air-dryer. Zeolites are commonly selected if it is intended to produce such an extremely low dew point dry air, as they often exhibit highly irreversible water isotherms, owning fairly large water adsorption amounts even at a very low water vapour pressure. By contrast, silica gels can adsorb larger water vapour than zeolites on the basis of unit adsorbent mass at relatively high vapour pressures. But they are deemed inferior to zeolites for producing a dry air of a very low dew point due to the isotherm being not as favourable as zeolites [1, 3, 4].

In Ahn and Lee's works[17, 18], a 13X column initially saturated with a water vapour at 12740 ppmv (54% relative humidity) was thermally regenerated by flowing a hot nitrogen gas through the column. The thermal regeneration experiments were carried out at a constant purge gas flowrate and three different temperatures, i.e. 423, 473 and 523K and the desorption experiment data were compared with the full numerical simulations as shown in Figure 1. The rate of the column being regenerated depends greatly on the temperature of the hot purge gas. We could save total usage of the

purge gas by flowing a hotter purge gas, or make use of a cooler purge gas by spending a larger amount of purge gas. However, it is uncertain at which temperature the thermal regeneration would be most efficient, taking into account the total energy consumption and the quality of heat determined by the temperature.

Meanwhile, an air-drying TSA process is often designed without having a cooling step between low-temperature adsorption step and high-temperature regeneration step due to the presence of a pure thermal wave, i.e. the temperature profile propagating ahead of the concentration profile during the adsorption step [1, 2]. In other words, the concentration profile of a water vapour in a 13X column in the adsorption step would not be affected by the initial bed temperature. In this case, the TSA cycle is configured so that the next adsorption step can be initiated immediately after the end of thermal regeneration step, shortening the cycle time to improve the bed productivity. Without a cooling step, the quality of a dry air produced in the beginning of the ensuing adsorption step would be affected greatly by the concentration of the water vapour remaining in the column after the thermal regeneration step. Therefore, it is crucial to regenerate the humid column very thoroughly during the thermal regeneration step to ensure to produce a dry air of an excellent quality even in the initial stage of adsorption step.

In this work, it is aimed to find the optimal hot purge gas temperature in regenerating thermally a 13X column saturated with water vapour at around 54% relative humidity. A preliminary guideline on selection of the optimal hot gas temperature is to be proposed by Equilibrium Theory, and subsequently validated by the full numerical simulation. Finally it will be shown that the ideal work consumption required for thermal regeneration lies at its minimum around the optimal hot gas temperature proposed by Equilibrium Theory.

## 2. Theory

### 2.1. Air-drying adsorption/thermal regeneration experiments and full numerical models

To simulate the dynamics of adsorption and thermal regeneration breakthrough, a set of mathematical equations of mass, energy and momentum balances around the adsorption column were constructed and discussed in details in the paper the author published recently [19]. Below are the balance equations taken for full numerical simulation of air-drying adsorption/thermal regeneration breakthrough.

Assuming the gas flow is a dispersed plug flow, a component mass balance is given by:

$$-\frac{\partial}{\partial z}\left(D_z \cdot c_T \frac{\partial y_i}{\partial z}\right)+\frac{\partial c_i}{\partial t}+\frac{\partial(u \cdot c_i)}{\partial z}+\frac{1-\varepsilon_b-\varepsilon_w}{\varepsilon_b}\cdot\frac{\partial \overline{q}_i}{\partial t}=0 \tag{1}$$

Along with the component mass balance, an overall mass balance needs to be solved for estimating the gas velocity that varies in both temporal and spatial domains.

$$\frac{\partial c_T}{\partial t}+\frac{\partial(u \cdot c_T)}{\partial z}+\frac{1-\varepsilon_b-\varepsilon_w}{\varepsilon_b}\cdot\sum_{i=1}^{n}\frac{\partial \overline{q}_i}{\partial t}=0 \tag{2}$$

Linear Driving Force (LDF) model was taken to estimate the adsorption rate.

$$\frac{\partial \overline{q}_i}{\partial t}=k_{LDF,i}\cdot(q_i^{*}-\overline{q}_i) \tag{3}$$

The energy balance equation is given by:

$$\begin{aligned}&(\hat{C}_{vg}\rho_g+\frac{1-\varepsilon_b-\varepsilon_w}{\varepsilon_b}\cdot\hat{C}_{ps}\rho_s+\frac{1-\varepsilon_b-\varepsilon_w}{\varepsilon_b}\cdot\hat{C}_{pg}\rho_{ads}+\frac{\varepsilon_w}{\varepsilon_b}\hat{C}_{pw}\rho_w)\frac{\partial T}{\partial t}-k_z\frac{\partial^2 T}{\partial z^2}\\&+\hat{C}_{vg}\rho_g u\cdot\frac{\partial T}{\partial z}-\frac{1-\varepsilon_b-\varepsilon_w}{\varepsilon_b}\cdot\sum_{i=1}^{n}(-\Delta H_i-RT)\frac{\partial \overline{q}_i}{\partial t}+\frac{\partial uP}{\partial z}+\frac{2h}{R_i}(T-T_w)=0\end{aligned} \tag{4}$$

As for the momentum balance, Ergun equation was taken to estimate the pressure

drop along the column length.

$$-\frac{dP}{dz}=\frac{150\cdot\mu\cdot u\cdot(1-\varepsilon)^2}{d_P^2\cdot\varepsilon^2}+\frac{1.75\cdot(1-\varepsilon)\cdot\rho_g\cdot u\cdot|u|}{d_P\cdot\varepsilon} \quad (5)$$

A generalised Toth isotherm was taken for estimating the equilibrium adsorption amount of water on zeolite 13X [20, 21].

$$q=\rho_p\frac{aRTc}{[1+(bRTc)^t]^{\frac{1}{t}}} \quad (6)$$

where a, b and t are a function of temperature as follows.

$$a=a_0e^{\frac{E}{T}} \quad (7)$$

$$b=b_0e^{\frac{E}{T}} \quad (8)$$

$$t=t_0+\frac{c}{T} \quad (9)$$

All the Toth isotherm parameters in Eqs. 6 – 9 were found in the references [20, 21] and listed in Table 1.

It is well known that the equilibrium adsorption isotherm of water on zeolite 13X exhibits capillary condensation with the water vapour pressure approaching its saturation pressure. To incorporate the effect of capillary condensation into the Toth isotherm, Eq. 6, Aranovich-Donohue (AD) model was applied as follows [22]:

$$q=\rho_p\frac{q_mbRTc}{[1+(bRTc)^t]^{\frac{1}{t}}\left(1-\frac{RTc}{P_S}\right)^d} \quad (10)$$

where $q_m$ and d are constant while b and t are a function of temperature as expressed in Eqs. 8 and 9. In this work, the $q_m$ and d were found and $b_0$ were re-estimated so that the A-D model could fit well the Toth isotherm, Eq. 6, in low vapour pressure regions. The three parameter values are listed in Table 1.

The water saturation pressure at a temperature, $P_s$, is estimated by Eq. 11.

$$P_s = 0.61094e^{17.625\frac{T-273.15}{T-30.11}} \quad (11)$$

Figure 2 shows the water vapour isotherms on zeolite 13X constructed with both Toth and AD models at 273, 298 and 373K. As can be seen, the capillary condensation effect is notable only in the region of relatively high water vapour pressures, approximately above the relative humidity of 50% [17].

The axial mass dispersion coefficient, $D_z$, and the axial thermal dispersion coefficient, $k_z$, are estimated using the correlations proposed by Wakao and Funazkri [23]:

$$\frac{\varepsilon \cdot D_z}{D_m} = 20 + 0.5 \cdot Sc \cdot \mathrm{Re} \quad (12)$$

$$\frac{k_z}{k_g} = 7 + 0.5 \cdot \mathrm{Pr} \cdot \mathrm{Re} \quad (13)$$

The boundary conditions at the column ends are given by Danckwerts boundary conditions expressed in the gas mole fraction and enthalpy [24]. The DAEs listed above were solved with gPROMS. The numerical solver was the second-order orthogonal collocation on finite elements with 200 nodes in the spatial domain. All the simulation parameters used in the full numerical simulation are listed in Tables 1 and 2.

In the past researches [17, 18, 25], a series of breakthrough experiments of adsorption followed by thermal regeneration were carried out. Before performing this experimental campaign, the adsorption column was thermally regenerated in situ at 593K at least for 12 hrs. Once the column is cooled down to 293K, an adsorption breakthrough run was initiated by feeding a gas mixture of water vapour and nitrogen carrier gas at 12740 ppm water (54 % relative humidity) at 9 NL/min. The water vapour concentration was measured by a hygrometer at the outlet of the column during the adsorption run. Once

the column was saturated with the feed, thermal regeneration breakthrough runs were performed by flowing a hot nitrogen at 26 NL/min at three different temperatures. As a result, the experimental breakthrough curves were obtained as shown in Figure 1. In this study, this adsorption system was analysed by a single component, non-isothermal adsorption model, assuming the carrier nitrogen gas would be inert on the grounds of the nitrogen adsorption amount being negligible compared to the water adsorption amount [26].

**Table 1.** List of adsorbent and column parameters taken for analysis of adsorption and thermal regeneration of water vapour on zeolite 13X fixed bed.

| ***Column parameters*** | |
|---|---|
| Column length [m] | 0.3 |
| Column diameter [m] | 0.033 |
| Column thickness [mm] | 2.3 |
| External bed void fraction, ε [-] | 0.37 |
| Wall density, $\rho_w$ [kg/m$^3$] | 7700 |
| Specific heat capacity of the wall, $C_{pw}$ [J/kg·K] | 500 |
| Overall heat transfer coefficient at the wall, h [W/m$^2$·K] | 1.5 |
| ***Gas and adsorbed phase parameters*** | |
| Axial mass dispersion coefficient, $D_z$ [m$^2$/s] | 2.316 $10^{-3}$ (ads) / 3.995 $10^{-3}$ (des) |
| Axial thermal dispersion coefficient, $k_z$ [W/m·K) | 2.766 (ads) / 3.374 (des) |
| Specific heat capacity of the gas, $C_{pg}$ [J/kg/K] | 1047 |
| Specific heat capacity of the adsorbed phase, $C_{pa}$ [J/kg·K] | 2392.6 |
| Gas viscosity, μ [Pa s] | 1.8 $10^{-5}$ |
| ***13X Zeolite parameters*** | |
| Adsorbent density, $\rho_s$ [kg/m$^3$] | 1100 |
| Specific heat capacity, $C_{ps}$ [J/kg/K] | 920 |
| Particle diameter, $d_p$ [mm] | 2.5 |
| $k_{LDF,CO2}$ [1/s] | 5.0 $10^{-4}$ (ads) / 5.0 $10^{-3}$ (des) |
| ***Toth Isotherm Parameters*** | |
| $a_0$ [mol/kg/kPa] | 3.634 $10^{-6}$ |
| $b_0$ [1/kPa] | 2.408 $10^{-7}$ |
| E [K] | 6,852 |
| - $\Delta H_{H2O}$ [J/mol] | 56,968 |
| $t_0$ [ - ] | 3.974 $10^{-1}$ |

| | |
|---|---|
| c [K] | -4.199 |
| ***Aranovich-Donohue (AD) Isotherm parameters*** | |
| $q_m$ [mol/kg] | 14.9 |
| $b_0$ [1/kPa] | $2.91\ 10^{-7}$ |
| d [ - ] | 0.03 |

**Table 2. Experimental conditions**.

| | |
|---|---|
| External/initial temperature [K] | 293 |
| Regeneration temperature [K] | 423 / 473 / 523 |
| Feed flowrate in the adsorption run [$Nm^3/s$] | $1.5\ 10^{-4}$ |
| Feed flowrate in the regeneration run [$Nm^3/s$] | $4.3\ 10^{-4}$ |
| Water vapour concentration in the adsorption run feed [$mol/m^3$] | 0.523 |
| Initial water vapour concentration in the column for adsorption run [$mol/m^3$] | $1.0\ 10^{-5}$ |

### 2.2. Equilibrium Theory model of an adiabatic, one adsorbing component plus inert carrier system

It is also possible to solve the mathematical models analytically with Equilibrium Theory [27, 28]. To this end, the full balance equations need to be simplified following the general assumptions involved in Equilibrium Theory. In addition, the enthalpy of the adsorbed phase was neglected in the energy balance, Eq. 4.

Accordingly the component mass balance and energy balance equations are simplified into Eqs. 14 and 15 as below.

$$\frac{\partial\left(\frac{y_i}{T}\right)}{\partial t}+\beta_i\frac{\partial\left(\frac{uy_i}{T}\right)}{\partial z}=0 \qquad (14)$$

where $\beta_i=\{1+[(1-\varepsilon)/\varepsilon](dq/dc)\}$[29].

$$\hat{C}_{vg}\rho_g u\cdot\frac{\partial T}{\partial z}+\left[\hat{C}_{vg}\rho_g+\frac{1-\varepsilon}{\varepsilon}\cdot\hat{C}_{ps}\rho_s-\frac{1-\varepsilon}{\varepsilon}\left(-\Delta H-RT\right)\frac{dq}{dT}\right]\frac{\partial T}{\partial t}+\frac{\partial uP}{\partial z}=0 \qquad (15)$$

The energy balance, Eq.15, can be expressed differently in terms of $C_p$ instead of $C_v$ as follows [19].

$$\hat{C}_{pg}\rho_g u\cdot\frac{\partial T}{\partial z}+\left[\hat{C}_{pg}\rho_g+\frac{1-\varepsilon}{\varepsilon}\cdot\hat{C}_{ps}\rho_s-\frac{1-\varepsilon}{\varepsilon}\left(-\Delta H\right)\frac{dq}{dT}\right]\frac{\partial T}{\partial t}=0 \qquad (16)$$

where the $\frac{\partial P}{\partial t}$ term is excluded as both adsorption and thermal regeneration must be a constant-pressure process.

Applying the method of characteristics [1] to Eq. 14 under the conditions of constant pressure and varying temperature, the concentration propagation velocity can be derived as:

$$w_C=\frac{u}{1+\frac{1-\varepsilon}{\varepsilon}\frac{dq}{dc}} \qquad (17)$$

The temperature propagation velocity is also derived by simply rearranging Eq. 16.

$$w_T=\frac{u}{1+\frac{1-\varepsilon}{\varepsilon}\frac{\hat{C}_{ps}\rho_s}{\hat{C}_{pg}\rho_g}-\frac{1-\varepsilon}{\varepsilon}\frac{-\Delta H}{\hat{C}_{pg}\rho_g}\frac{dq}{dT}} \qquad (18)$$

By summing the two component mass balance equations, Eq. 14, for water (A) and nitrogen (B), the gas velocity can be estimated by:

$$\frac{\partial\left(\frac{u}{T}\right)}{\partial z}=\frac{1}{T^2\beta_B\left[1+\left(\beta-1\right)y_A\right]}\frac{\partial T}{\partial t}-\frac{u\left(\beta-1\right)}{T\left[1+\left(\beta-1\right)y_A\right]}\frac{\partial y_A}{\partial z} \qquad (19)$$

where $\beta=\beta_A/\beta_B$[29].

For the system considered in this study, Eq. 19 can be simplified by taking $\beta = \beta_A = 0$ and $\beta_B = 1$, given the assumptions that water is a strongly adsorbing component and the nitrogen carrier gas is inert. Also it was assumed that the temperature variation with

time would be neglected. In the limiting case, Eq. 19 becomes:

$$\frac{u}{u_0} = \frac{T}{T_0}\frac{\left(1-y_A\right)}{\left(1-y_{A0}\right)} \tag{20}$$

Coherence rule has to be met for the two propagation velocities [1, 2, 27]. Equating the two equations, Eqs. 17 and 18, results in a quadratic equation, Eq.21.

$$\frac{dc}{dT} = \frac{-\left(\frac{\partial q}{\partial c}-\frac{\widehat{C}_{ps}\rho_s}{\widehat{C}_{pg}\rho_g}+\frac{-\Delta H}{\widehat{C}_{pg}\rho_g}\frac{\partial q}{\partial T}\right)\pm\sqrt{\left(\frac{\partial q}{\partial c}-\frac{\widehat{C}_{ps}\rho_s}{\widehat{C}_{pg}\rho_g}+\frac{-\Delta H}{\widehat{C}_{pg}\rho_g}\frac{\partial q}{\partial T}\right)^2-4\frac{\partial q}{\partial T}\frac{-\Delta H}{\widehat{C}_{pg}\rho_g}\frac{\partial q}{\partial c}}}{2\frac{-\Delta H}{\widehat{C}_{pg}\rho_g}\frac{\partial q}{\partial c}} \tag{21}$$

Solving the quadratic equation provides two real roots: one is positive and the other is negative. By substituting each of two dc/dT values into Eqs. 17 and 18, the location of a plateau being placed between the initial and feed states can be identified. At the same time, it has to be checked if the two transitions occurring around the plateau is either shock or simple wave. If a shock wave is to be formed, the velocities of concentration and temperature shock fronts are given by:

$$w_C = \frac{u}{1+\frac{1-\varepsilon}{\varepsilon}\frac{\Delta q}{\Delta c}} \tag{22}$$

$$w_T = \frac{u}{1+\frac{1-\varepsilon}{\varepsilon}\frac{\widehat{C}_{ps}\rho_s}{\widehat{C}_{pg}\rho_g}-\frac{1-\varepsilon}{\varepsilon}\frac{-\Delta H}{\widehat{C}_{pg}\rho_g}\frac{\Delta q}{\Delta T}} \tag{23}$$

## 3. Results and discussion

### 3.1. Adsorption breakthrough analysis

Firstly, the hodograph for adsorption breakthrough profiles was constructed as shown in Figure 3(a). In the adsorption breakthrough, the state of the adsorption column changes with time from initial clean state (concentration [mol/$m^3$]: temperature [K] = $10^{-5}$: 293), to feed state (0.523, 293) via intermediate state (5.5 $10^{-5}$, 318.2). It should be noted that the negative characteristic of the feed state must be a shock wave rather than a simple wave, hence the intermediate state had to be found where the following two lines intersect each other: positive characteristic of the initial state (simple wave) and negative characteristic of the feed state (shock wave). Based on the hodograph, the concentration and temperature profiles (dashed line) were constructed as shown in Figure 3(b). Only one transition of the concentration profile appears, as the concentration change is negligible along the route from the initial state to the intermediate state on the hodograph. By contrast, two temperature transitions show up, resulting in this adsorption system being characterised by a pure thermal wave. The existence of a pure thermal wave was also checked by comparing the pure thermal wave velocity and the isothermal concentration wave velocities under two limiting conditions, i.e. the feed temperature (slowest) or the maximum plateau temperature (fastest) [30].

Subsequently, the Equilibrium Theory model was solved numerically by gPROMS. Ideally, the axial and thermal dispersion coefficients must be set zero and the LDF constant must be set close to infinity to mimic the Equilibrium Theory model. To ensure convergence of the solver, however, both $D_z$ and $k_z$ decreased 10 times smaller than the actual and the LDF constant increased 10 times larger. The c and T profiles estimated by solving numerically the Equilibrium Theory model (not shown in Figure 3b) were in a good agreement with those by hodograph, while slight discrepancy of the two was inevitable due to the numerical model still accommodating the effects of the diffusion-related terms. Figure 3 also contains the experimental data and their

associated full numerical simulation result. As can be seen, the two first moments of the breakthrough curves constructed by Equilibrium Theory and full numerical simulation were fairly close to each other, evidencing the validity of the Equilibrium Theory model taken in this study.

### 3.2. Determination of optimal hot purge gas temperature in thermal regeneration

As for thermal regeneration of the adsorption column saturated with water vapour, a hodograph was also constructed at three different temperatures of a hot purge gas in a range of 423K to 523K as shown in Figure 4(a). It is worth investigating the location of the watershed point, to ensure that the hot purge temperatures be chosen below the watershed point. Increasing the purge temperature above the watershed point could not but result in greater energy consumption, as it could not shorten the time taken for thermal regeneration [1]. To find the watershed point, it is necessary to evaluate Eq. 21 under the condition of the concentration approaching zero. The two derivatives, $\frac{\partial q}{\partial c}$ and $\frac{\partial q}{\partial T}$, at c = 0 become:

$$\left(\frac{\partial q}{\partial c}\right)_{c=0} = \rho_p aRT \quad (24)$$

$$\left(\frac{\partial q}{\partial T}\right)_{c=0} = 0 \quad (25)$$

Then, the watershed temperature can be found so as to meet $\rho_p aRT = \frac{C_s}{C_f}$. In this water vapour-13X system, The watershed point was estimated 603.534 K for water vapour adsorption on 13X, indicating the purge gas temperatures (423 – 523K) taken in this study are worth investigating, as they are far below the watershed point.

In scrutinizing the negative characteristics of the feed state in Figure 4(a), it can be observed that the two plots at 473 and 523 K exhibit their slopes alternating increasing and decreasing with temperature, while the slope of the plot at 423K increases monotonously over the entire range. The slopes of the characteristics, dT/dc, were plotted at different temperatures in Figure 4(b) in which horizontal lines were added to show at which value the area enveloped by each plot is divided equally. It should be noted that the fraction of the plot occupied by the horizontal line becomes larger with

temperature. Such interesting trends of the characteristics are attributed to the Toth adsorption isotherm chosen in this study.

In Figure 5, the c and T breakthrough curves (red dots) were constructed at the three hot purge gas temperatures based on the hodography in Figure 4(a). The two transitions of concentration and temperature were clearly observed in accordance with the hodography. As the feed temperature increases, the concentration plateau between the two transitions, in other words a roll-up of concentration by temperature, is formed at a higher concentration. It is notable that the trailing profile exhibits different shapes with temperatures, in accordance with the change of the slope of dT/dc presented in Figure 4(b). At 423K the c and T profiles are a simple wave, changing monotonously throughout the entire range, whilst at 473 and 523K they are initially a simple wave in the high concentration region, similarly to the 423K profile, but they move in the opposite direction. The profiles revert to simple wave at low concentrations, approaching to the feed state.

However, such c and T profiles constructed by the hodograph at 473 and 523K are existent only theoretically. It was presumed that the actual profiles would be shock wave rather than curved line in the region where a vertical line divides equally the area enveloped by the c or T curves. The mathematical models used in Equilibrium Theory were solved numerically with large LDF constant and reduced Dz and kz. The numerical results (black lines) corroborated the presumption well.

From the c and T profiles at the three temperatures, it can be observed that the portion that the shock wave occupies along the trailing front becomes larger with increasing temperature. At 473K, the shock wave is less prominent, so that the simple wave following the shock wave is still visible at the low concentrations, indicating that it would take long to regenerate the column rigorously. At 523K, however, the trailing front is almost completely occupied by the shock wave, enabling the adsorption column to be

regenerated fast and efficiently.

In Figure 6, the concentration range of the trailing front occupied by the shock wave were quantified by drawing horizontal lines dividing equally the areas enveloped by the profiles. It should be noted that the ranges of the shock waves denoted by the dashed lines are different from those estimated by dT/dc in Figure 4(b), as the gas velocity is not constant but varies with temperature and composition (see Eq. 20).

As discussed above, the existence of a shock front implies that an adsorption column would be regenerated more efficiently within the concentration range covered by the shock wave. And the range of the concentration occupied by a shock front is highly dependent on the hot purge gas temperature. As shown in Figure 6, the lower bound of the concentration range directed by the horizontal line decreases with increasing hot purge gas temperature. In other words, the adsorption column has to be regenerated by a hotter purge gas, if it is intended to regenerate it more rigorously.

Figure 7 shows the upper and lower bounds of each shock wave in the temperature range from 473 to 523K. The lower bound of the shock wave is equivalent to the minimum water vapour remaining in the column achievable by efficient thermal regeneration at a given purge gas temperature. Subsequently, the water vapour concentration at the lower bound was converted into its dew point. Finally, a correlation was found to relate the minimum dew point achievable by efficient thermal regeneration with the hot purge gas temperature as follows.

$$\mathrm{DP}\,[^{\circ}\mathrm{C}] = -0.012\mathrm{T}[\mathrm{K}]^2 + 10.702\mathrm{T}[\mathrm{K}] - 2385 \qquad (26)$$

### 3.3. Effect of capillary condensation

Up to this point, the adiabatic, single-component advection equations were solved with the Toth isotherm model, without considering the effect of capillary condensation taking place at relatively high water vapour pressure. The effect of capillary condensation must be taken into account in thermal regeneration, whilst its effect is often neglected in case of adsorption breakthrough if the water vapour pressure in the feed is far less than the saturation pressure [17]. This is due to the desorbed water vapour being re-adsorbed in the region of column that was not fully heated yet. In the part of the column where re-adsorption occurs, the water vapour pressure may go over its pressure in the feed to an extent of enabling capillary condensation. To see the effect of capillary condensation, the Equilibrium Theory models were solved numerically with the Aranovich-Donohue isotherm model combined with Toth model, Eq. 10, and the results are presented in Figure 8. Compared to the profiles estimated with Toth isotherm only, the new profiles shows clearly that the plateaus of concentration and temperature were extended significantly at 423 and 473K. At 523K, the region of the shock wave was so dominant that it was combined with the plateau extended by capillary condensation. It should be noted that the shape of the simple wave appearing after the shock wave was rarely affected by capillary condensation, as the effect of capillary condensation would occur only in the region of relatively high water vapour pressures. As a result, the optimal hot purge gas temperatures estimated with Toth isotherm are still valid even in the case where capillary condensation effect is taken into account.

### 3.4. Validation of the proposed optimal hot purge gas temperature

The full mathematical models, Eqs. 1 to 13, were solved numerically to simulate the thermal regeneration breakthroughs at different purge gas temperatures in the range of 423 to 543K in the interval of 10K. In Figure 9, the simulation results were plotted along with the experimental data. As expected, the times taken for thermal regeneration to the same extent do not increase at constant intervals when the purge gas temperature decreases by 10K. On the contrary, the increment of the regeneration time increases notably when the purge gas temperature decreases below the proposed optimal value. At -40 °C of the dew point, for example, the increments of the required regeneration time were almost identical up to 513 K at which temperature the minimum dew point was still below -40 C as seen in Figure 7. By contrast, the regeneration time increased greatly with decreasing purge gas temperature from 503 K onwards at which temperatures simple waves prevail at the low concentration of water vapour. Therefore the hot purge gas temperature must be at least 513 K or higher for efficient thermal regeneration if it is intended to regenerate the column to the dew point of -40 °C. Likewise, the hot purge gas temperature must be at least 503 K or 493 K for the dew points of -30 °C or -20 °C, respectively.

It is interesting to see the effect of the purge gas temperature on the total energy consumption resulting from flowing the hot nitrogen gas in regenerating a humid column to the same extent. A humid column could be regenerated more quickly by flowing a hotter purge gas that is of higher quality, while it would be regenerated by flowing a low-grade, cooler gas at the expense of greater usage of purge gas. Figure 10 shows the thermal energy consumption varying with the hot purge gas temperature, based on the times taken for thermal regeneration up to the dew point of -40 °C estimated by full numerical simulation presented in Figure 9. As can be seen, the heat energy consumption increases rapidly with decreasing temperature. Due to large

difference of the required regeneration times between the cases, the higher the purge gas temperature is, the smaller the total energy consumption becomes.

However, the total energy consumption estimated in terms of simply enthalpy cannot take into account the quality of a hot purge gas determined by its temperature, in other words, ignoring the fact that a high temperature gas is more valuable than a low temperature gas. In order to consider properly the quality of the thermal energy, the concept of an ideal work achievable from ideal conversion of a heat, also known as exergy, was taken to quantify the energy consumption more sensibly as follows.

$$W_{id} = \dot{m}\Delta t\left(\Delta\dot{H} - T_0\Delta\dot{S}\right) \quad (27)$$

Figure 10 shows clearly the total ideal work consumption being at its minimum around 513K, corroborating the finding of the optimal purge gas temperature estimated by Equilibrium Theory approach.

## 4. Conclusions

The thermal regeneration of a humid 13X adsorption column by flowing a hot purge gas was studied by Equilibrium Theory analysis. As a result, it was found out that the hot purge gas temperature must be selected carefully depending on the targeted water vapour concentration remaining in the column after thermal regeneration. The findings of this research paves the way for optimising an air-drying TSA process, as regenerating thermally a humid column with a hot purge gas at the proposed optimal temperature can shorten the cycle time and minimise the ideal work consumption simultaneously.

**Nomenclature**

| | |
|---|---|
| $a$ | Toth isotherm parameter, Eq. 6 (mol/kg/kPa) |
| $a_0$ | Toth isotherm parameter, Eq. 7 (mol/kg/kPa) |
| $b$ | Toth isotherm parameter, Eq. 6 (1/kPa) |
| $b_0$ | Toth isotherm parameter, Eq. 8 (1/kPa) |
| $c$ | Toth isotherm parameter, Eq. 9 (K) |
| $c_i$ | Component concentration (mol/m$^3$) |
| $c_T$ | Total concentration (mol/m$^3$) |
| $\hat{C}_{pa}$ | Specific adsorbed phase heat capacity (J/kg/K) |
| $\hat{C}_{vg}$, $\hat{C}_{pg}$ | Specific gas heat capacity (J/kg/K) |
| $\hat{C}_{ps}$ | Specific adsorbent heat capacity (J/kg/K) |
| $\hat{C}_{pw}$ | Specific wall heat capacity (J/kg/K) |
| $d$ | Aranovich-Donohue isotherm parameter, Eq. 10 (-) |
| $D_m$ | Molecular diffusivity (m$^2$/s) |
| $D_z$ | Axial dispersion coefficient (m$^2$/s) |
| $d_p$ | Adsorbent diameter (m) |
| $E$ | Toth isotherm parameter, Eqs. 7 and 8 (K) |
| $\Delta\dot{H}$ | Difference of the specific enthalpies of the two stream (kJ/kg) |
| $-\Delta H$ | heat of adsorption (J/mol) |
| $h$ | overall heat transfer coefficient at the wall (W/m$^2$/K) |
| $k_g$ | Gas thermal conductivity (W/m/K) |
| $k_{LDF}$ | LDF parameter (1/s) |
| $k_z$ | Axial thermal dispersion (W/m/K) |
| $\dot{m}$ | Mass flow rate (kg/s) |
| $P$ | Pressure (kPa) |
| $Pr$ | Prandtl number (-) |
| $P_s$ | Saturation pressure (kPa) |
| $\bar{q}$, $q$ | Adsorbed amount (mol/m$^3$) |
| $q_m$ | Aranovich-Donohue isotherm parameter, Eq. 10 (mol/kg) |
| $R$ | universal gas constant (kPa·m$^3$/mol/K) |
| $Re$ | Reynolds number (-) |
| $Sc$ | Schmidt number (-) |
| $\Delta\dot{S}$ | Difference of the specific entropies of the two streams (kJ/kg/K) |
| $T$ | Temperature (K) |
| $T_0$ | Ambient temperature (K) |
| $t$ | time (s) or Toth isotherm parameter, Eq. 6 (-) |
| $\Delta t$ | Time taken for thermal regeneration (s) |
| $t_0$ | Toth isotherm parameter, Eq. 9 (-) |
| $u$ | Gas velocity (m/s) |
| $V$ | Volume (m$^3$) |
| $W_{id}$ | Total ideal work (kJ) |
| $w_c$ | Concentration propagation velocity (m/s) |
| $w_T$ | Temperature propagation velocity (m/s) |
| $y_i$ | Gas mole fraction (-) |
| $z$ | Axial direction (m) |
| Greek Letters | |
| $\varepsilon$ | Bed void fraction (-) |

| | |
|---|---|
| $\varepsilon_b$ | Void fraction of bed internal over the entire column volume (-) |
| $\varepsilon_w$ | Fraction of volume of the wall over the entire column (-) |
| $\mu$ | Viscosity (Pa·s) |
| $\rho_s$ | Adsorbent density (kg/m$^3$) |
| $\rho_g$ | Gas density (kg/m$^3$) |
| $\rho_{ads}$ | Adsorbed phase density (kg/m$^3$) |
| $\rho_w$ | Column wall density (kg/m$^3$) |
| Subscripts | |
| *i* | Component i |
| *0* | Feed condition |
| Abbreviation | |
| c | Concentration |
| T | Temperature |
| DP | Dew Point |
| AD | Aranovich-Donohue |
| TSA | Thermal Swing Adsorption |

## References


[1] D.M. Ruthven, Principles of Adsorption and Adsorption Processes, John Wiley & Sons, Inc., 1984.

[2] R.T. Yang, Gas Separation by Adsorption Processes, Imperial College Press, 1997.

[3] J. Nastaj, B. Ambrozek, Analysis of Gas Dehydration in TSA System with Multi-layered Bed of Solid Adsorbents, Chemical Engineering and Processing: Process Intensification, 96 (2015) 44 - 53.

[4] P. Zhang, L. Wang, Numerical Analysis on the Performance of the Three-Bed Temperature Swing Adsorption Process for Air Prepurification, Industrial & Engineering Chemistry Research, 52 (2013) 885 - 898.

[5] E. Gabrus, K. Witkiewicz, J. Nastaj, Modeling of Regeneration Stage of 3A and 4A Zeolite Molecular Sieves in TSA Process Used for Dewatering of Aliphatic Alcohols, Chemical Engineering, 337 (2018) 416 - 427.

[6] M. Djaeni, P. Bartels, J. Sanders, G. van Straten, A.J.B. van Boxtel, Process Integration for Food Drying with Air Dehumidified by Zeolites, Dyring Technology, 25 (2007) 225-239.

[7] A. Anbarasan, J. Nataraj, N. Shanmukhan, A. Radhakrishnan, Effect of Hygroscopicity on Pharmaceutical Ingredients, Methods to Determine and Overcome: An Overview, Journal of Chemical and Pharamceutical Research, 10 (2018) 61 - 67.

[8] C. Ratti, Hot Air and Freeze-drying of High-value Foods: A Review, Journal of Food Engineering, 49 (2001) 311 - 319.

[9] Validation of System for Air Quality. http://rastgar-co.com/air-quality/ (accessed 16/04/19).

[10] D. White, Regenerative Desiccant Compressed Air Dryers. https://www.airbestpractices.com/technology/air-treatmentn2/regenerative-desiccant-

compressed-air-dryers (accessed 16/04/19).
[11] H. Lou, H. Miyajima, F. Dong, A. Kodama, M. Goto, T. Hirose, Experimental Study of Thermal Phenomenon in PSA Air Dehumidification, Separation and Purification Technology, 17 (1999) 65 - 75.
[12] S.U. Rege, R.T. Yang, K. Qian, M.A. Buzanowski, Air-Prepurification by Pressure Swing Adsorption Using Single/Layered Beds, Chemical Engineering Science, 56 (2001) 2745 - 2759.
[13] K. Chihara, M. Suzuki, Air Drying by Pressure Swing Adsorption, Journal of chemical Engineering of Japan, 16 (1983) 293 - 299.
[14] P. Zhang, L. Wang, Comparative Study on the Performance of Adsorbent Bed Regenerated by the Clean and Used Purge Gas Heating, Industrial & Engineering Chemistry Research, 52 (2013) 15915 - 15922.
[15] M. Djaeni, P.V. Bartels, J.P.M. Sanders, G. van Straten, A.J.B. van Boxtel, Computational Fluid Dynamics for Multistage Adsorption Dryer Design, Dyring Technology, 26 (2008) 487 - 502.
[16] J.A. Wurzbacher, C. Gebald, N. Piatkowski, A. Steinfeld, Concurrent Separation of CO2 and H2O from Air by a Temperature-Vacuum Swing Adsorption/Desorption Cycle, Environmental Science & Technology, 46 (2012) 9191-9198.
[17] H. Ahn, C.-H. Lee, Effects of Capillary Condensation on Adsorption and Thermal Desorption Dynamics of Water in Zeolite 13X and Layered Beds, Chemical Engineering Science, 59 (2004) 2727 - 2743.
[18] H. Ahn, C.-H. Lee, Adsorption Dynamics of Water in Layered Bed for Air-drying TSA Process, AIChE Journal, 49 (2003) 1601 - 1609.
[19] M. Luberti, Y.-H. Kim, C.-H. Lee, M.-C. Ferrari, H. Ahn, New Momentum and Energy Balance Equations Considering Kinetic Energy Effect for Mathematical Modelling of a Fixed-bed Adsorption Column, Adsorption, 21 (2015) 353 - 363.
[20] Y. Wang, M.D. LeVan, Adsorption Equilibrium of Carbon Dioxide and Water Vapor on Zeolites 5A and 13X and Silica Gel: Pure Component, Journal of Chemical & Engineering Data, 54 (2009) 2839-2844.
[21] Y. Wang, M.D. LeVan, Adsorption Equilibrium of Binary Mixtures of Carbon Dioxide and Water Vapor on Zeolites 5A and 13X, Journal of Chemical & Engineering Data, 55 (2010) 3189 - 3195.
[22] K.-Y. Kim, H.-T. Oh, S.-J. Lim, K. Ho, Y. Park, C.-H. Lee, Adsorption Equilibria of Water Vapor on Zeolite 3A, Zeolite 13X, and Dealuminated Y Zeolite, Journal of Chemical & Engineering Data, 61 (2016) 1547 - 1554.
[23] N. Wakao, T. Funazkri, Effect of Fluid Dispersion Coefficients on Particle-to-fluid Mass Transfer Coefficients in Packed Beds, Chemical Engineering Science, 33 (1978) 1375 - 1384.
[24] M. Luberti, G.D. Oreggioni, H. Ahn, Design of a Rapid Vacuum Pressure Swing Adsorption (RVPSA) Process for Post-Combustion $CO_2$ Capture from a Biomass-fuelled CHP

Plant, Journal of Environmental Chemical Engineering, 5 (2017) 3973 - 3982.
[25] H. Ahn, Adsorption and Thermal Regeneration of Water in a Fixed-bed of Air-drying TSA Process, in, Yonsei University, 2002.
[26] H. Deng, H. Yi, X. Tang, Q. Yu, P. Ning, L. Yang, Adsorption Equilibrium for Sulhur Dioxide, Nitric Oxide, Carbon Dioxide, Nitrogen on 13X and 5A Zeolites, Chemical Engineering Journal, 188 (2012) 77 - 85.
[27] H.-K. Rhee, R. Aris, N.R. Amundson, First-Order Partial Differential Equations: Vol.1 Theory and Application of Single Equations, Dover Publications, INC., 1986.
[28] H.-K. Rhee, R. Aris, N.R. Amundson, First-Order Partial Differential Equations: Vol.2 Theory and Application of Hyperbolic Systems of Quasilinear Equations, Dover Publications, INC., 1989.
[29] D.M. Ruthven, S. Farooq, K.S. Knaebel, Pressure Swing Adsorption, Wiley-VCH, 1993.
[30] C.-Y. Pan, D. Basmadjian, An Analysis of Adiabatic Sorption of Single Solutes in Fixed Beds: Pure Thermal Wave Formation and Its Practical Implications, Chemical Engineering Science, 25 (1970) 1653 - 1664.

Figure

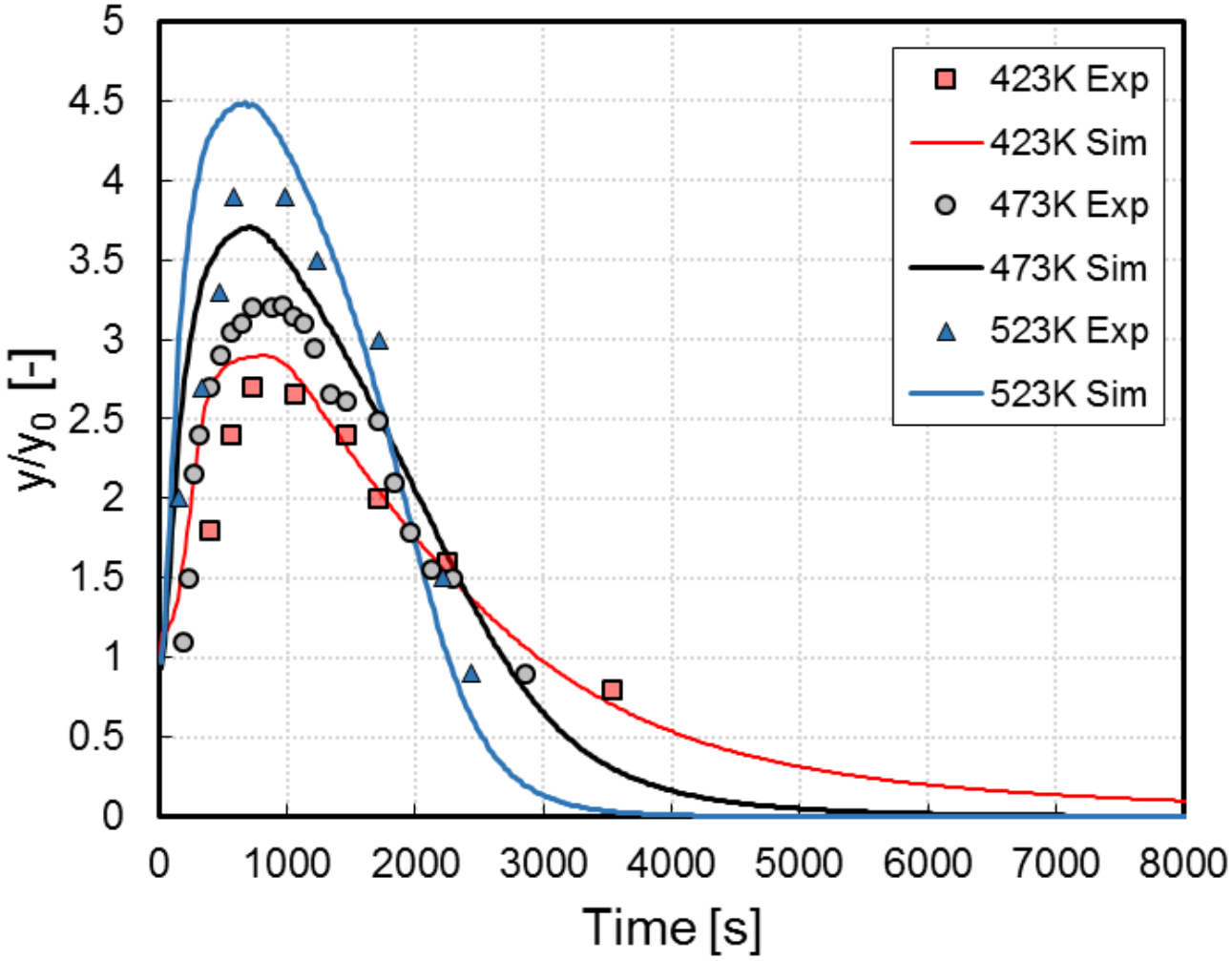


Figure 1. Effect of the hot nitrogen temperature on thermal regeneration breakthroughs of a 13X column initially saturated with water vapour at 12740 ppmv at 423K, 473K and 523K (Experimental data from Ref. [17]).

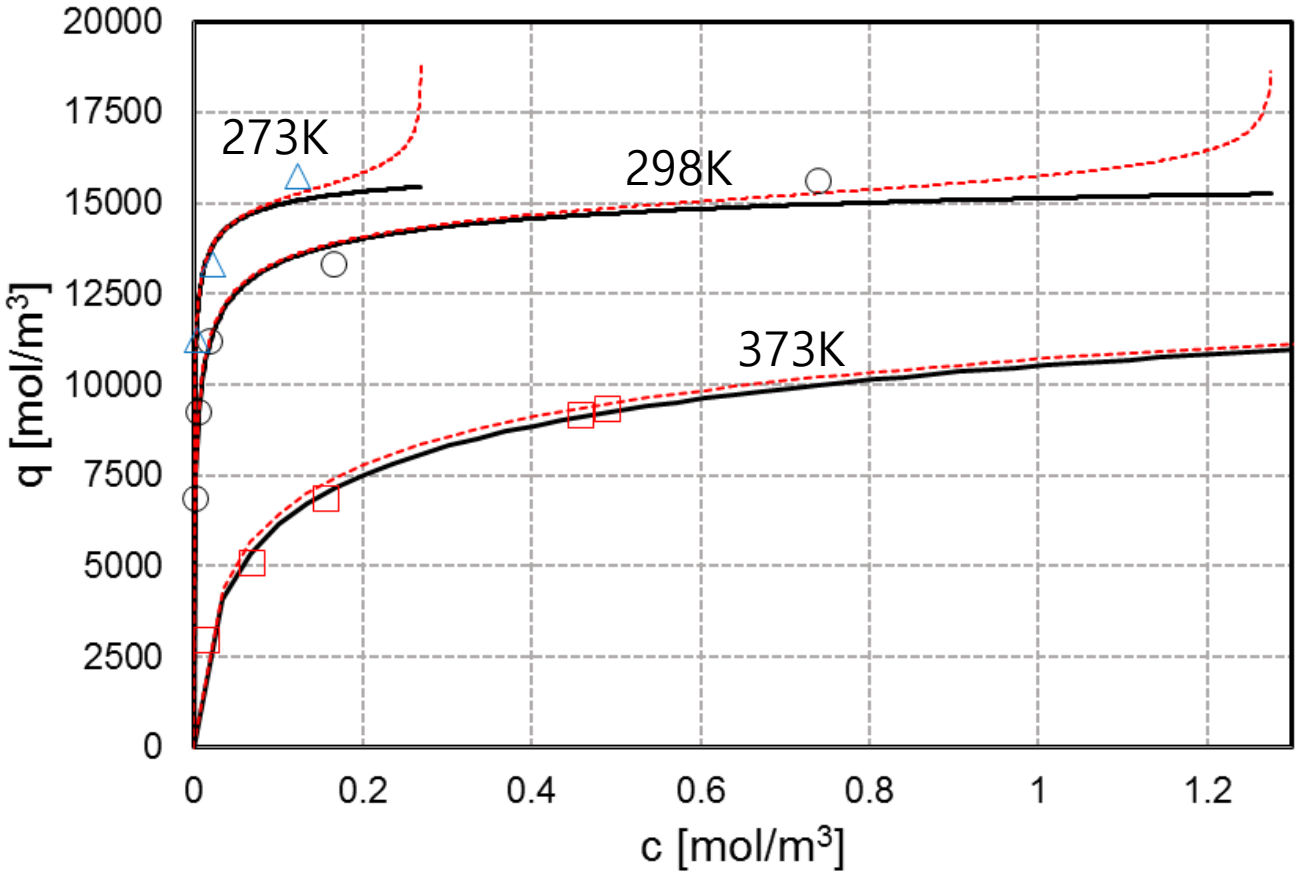


Figure 2. Adsorption isotherms of water vapour on zeolite 13X at 273, 298 and 373K (black full line: Toth, red dashed line: Aranovich-Donohue with Toth, symbols: experimental data from Ref. [20]).

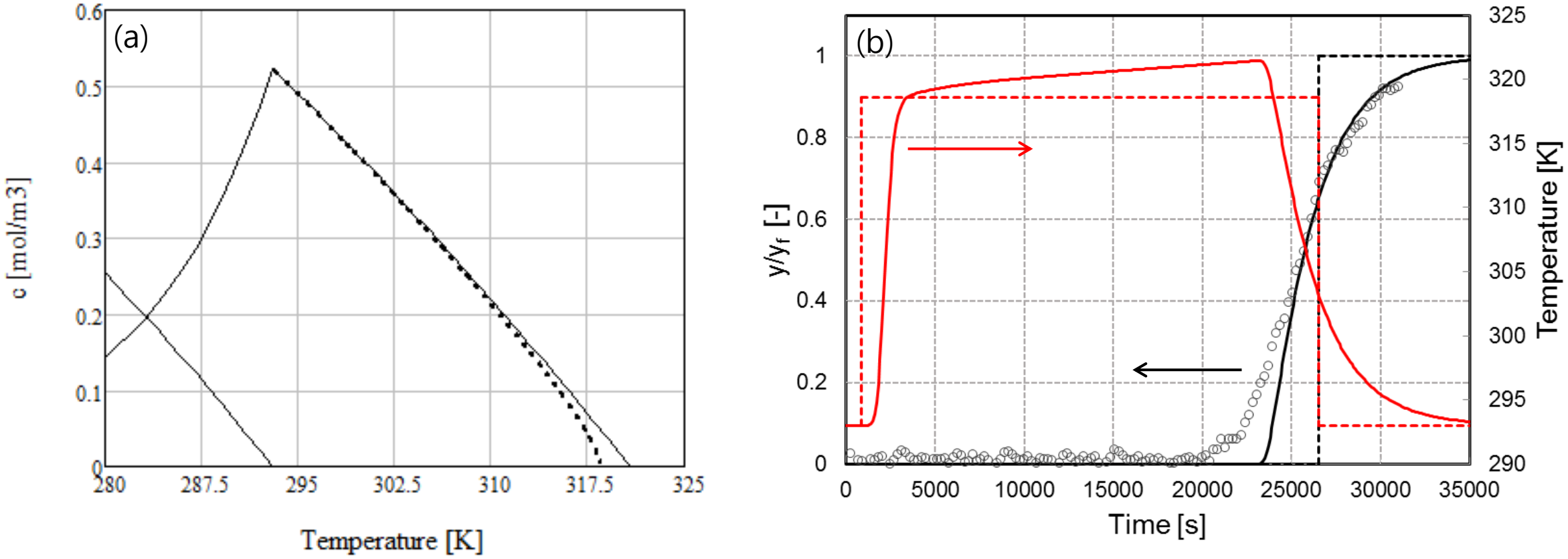


Figure 3. Adsorption breakthrough of water vapour (12740 ppmv) in zeolite 13X column at 293K: (a) Hodograph plane and (b) water mole fraction and temperature profiles constructed by hodograph (dashed lines) and full numerical simulation (solid lines) (experimental data from Ref. [17]).

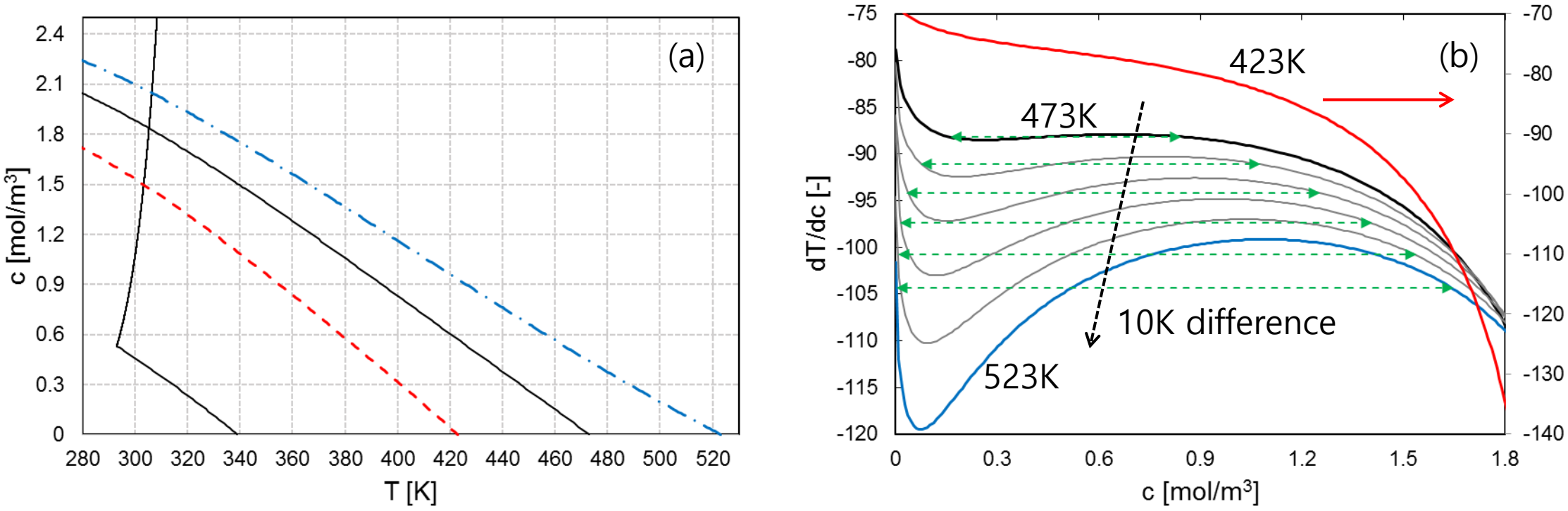


Figure 4. (a) Hodograph plane of thermal regeneration of a zeolite 13X column initially saturated with 12740 ppmv water vapour by a hot purge gas at 423, 473 and 523K and (b) dT/dc plots at temperature varying from 423 to 523K.

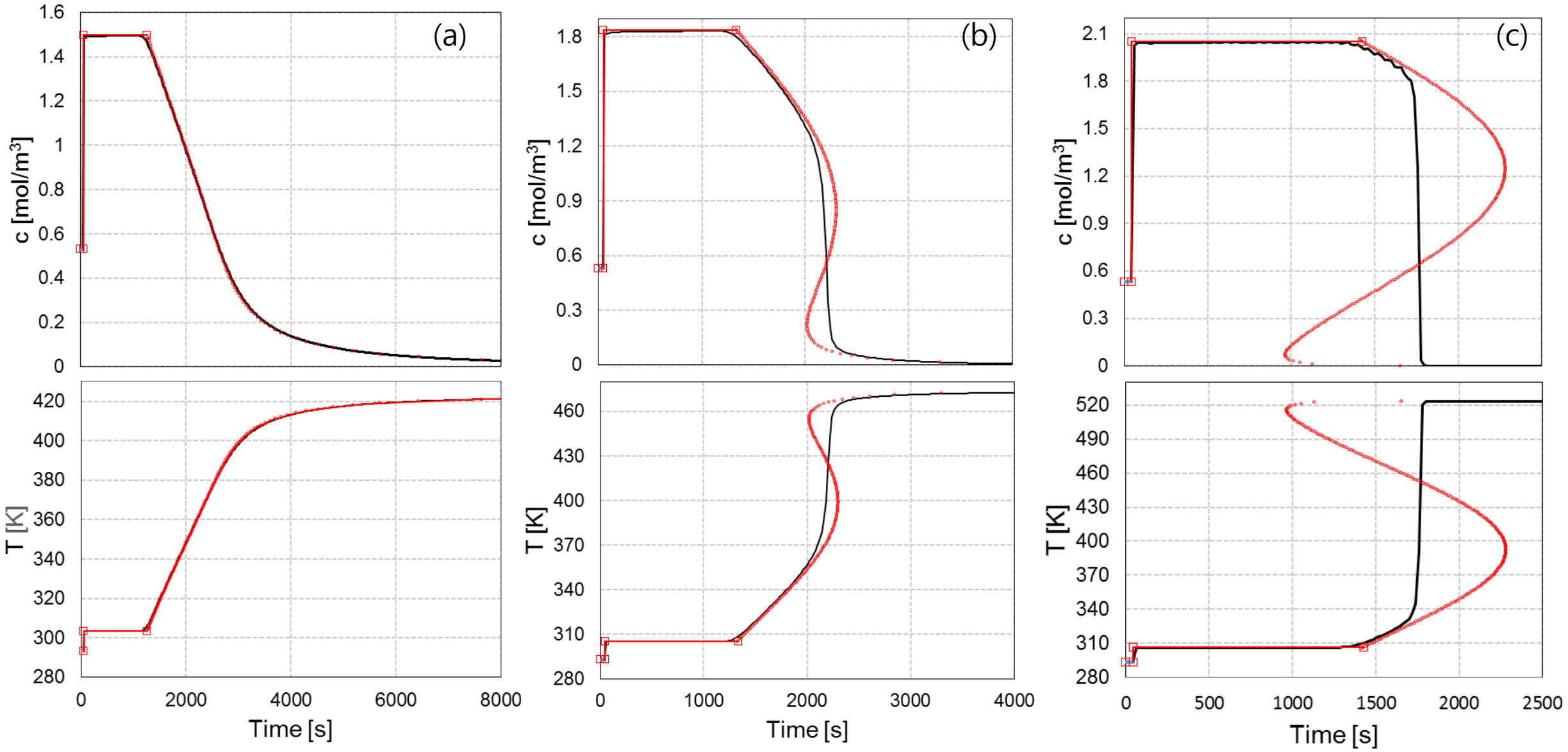


Figure 5. Water vapour concentration and temperature profiles at the column outlet constructed by Equilibrium Theory at (a) 423K, (b) 473K and (c) 523K.

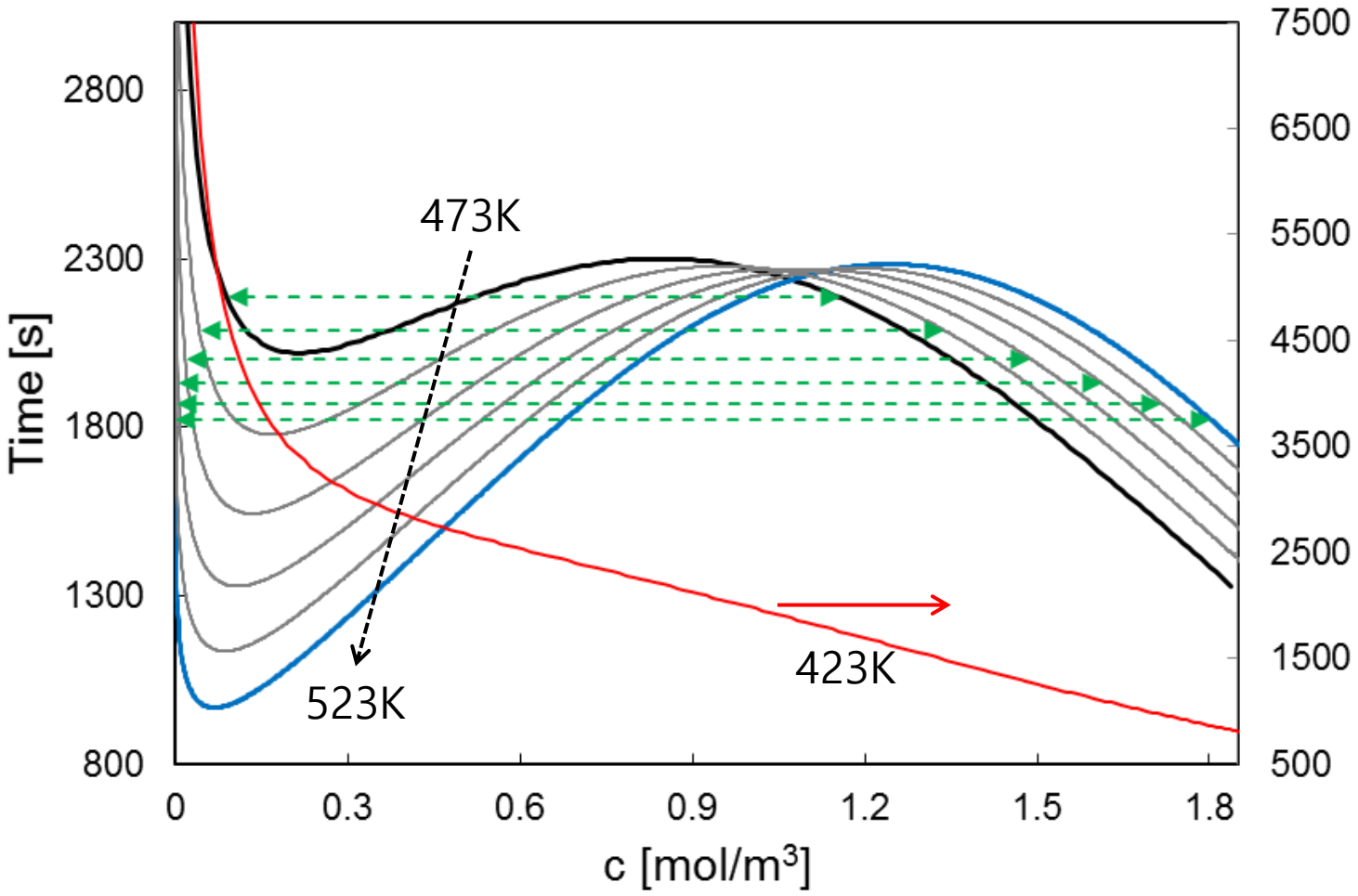


Figure 6. Shock wave locations of the regeneration breakthrough curves from 473K to 523K in the interval of 10K.

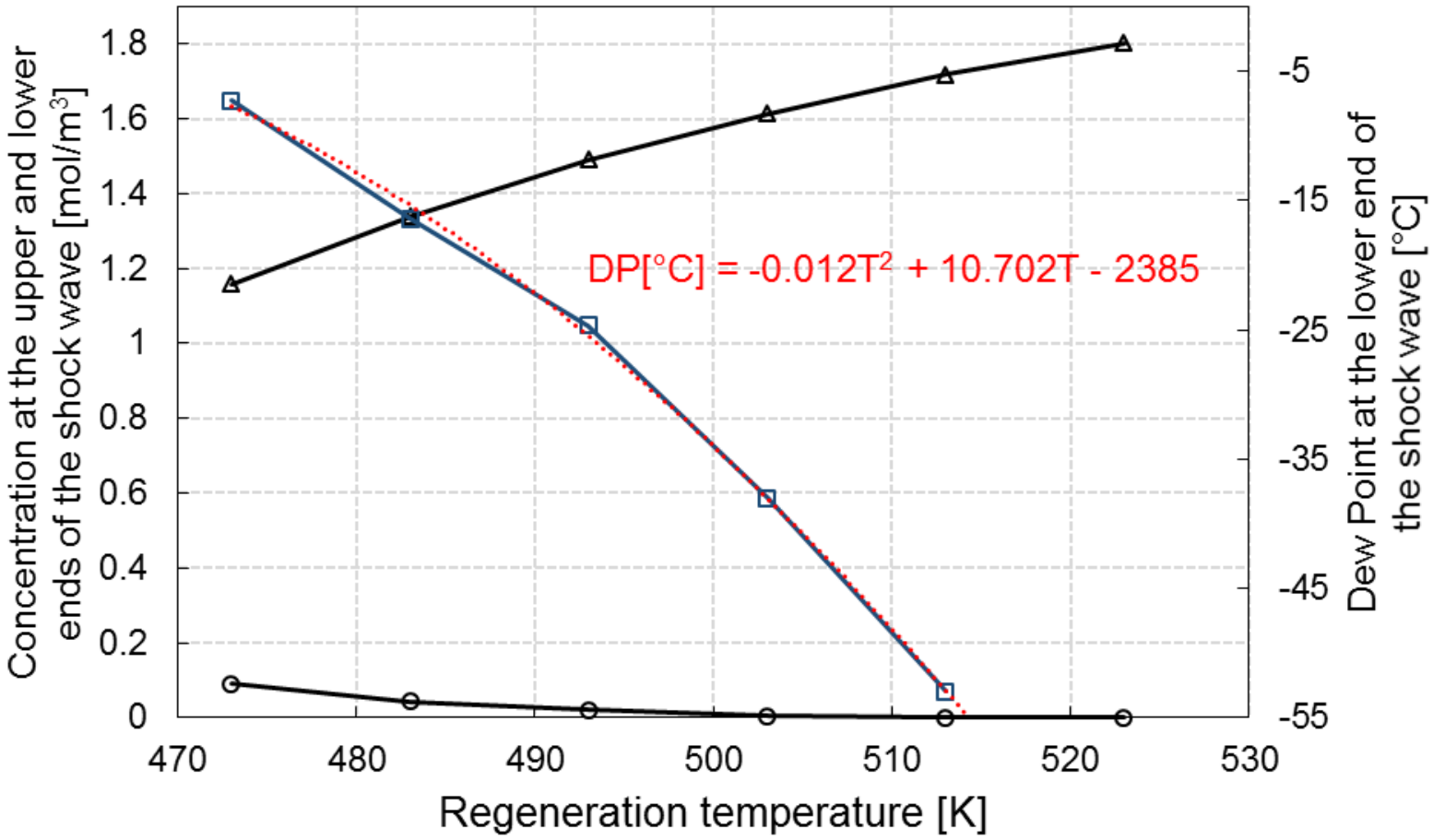


Figure 7. Optimal regeneration temperature determined by the lower end of the shock wave at temperatures varying from 473K to 523K.

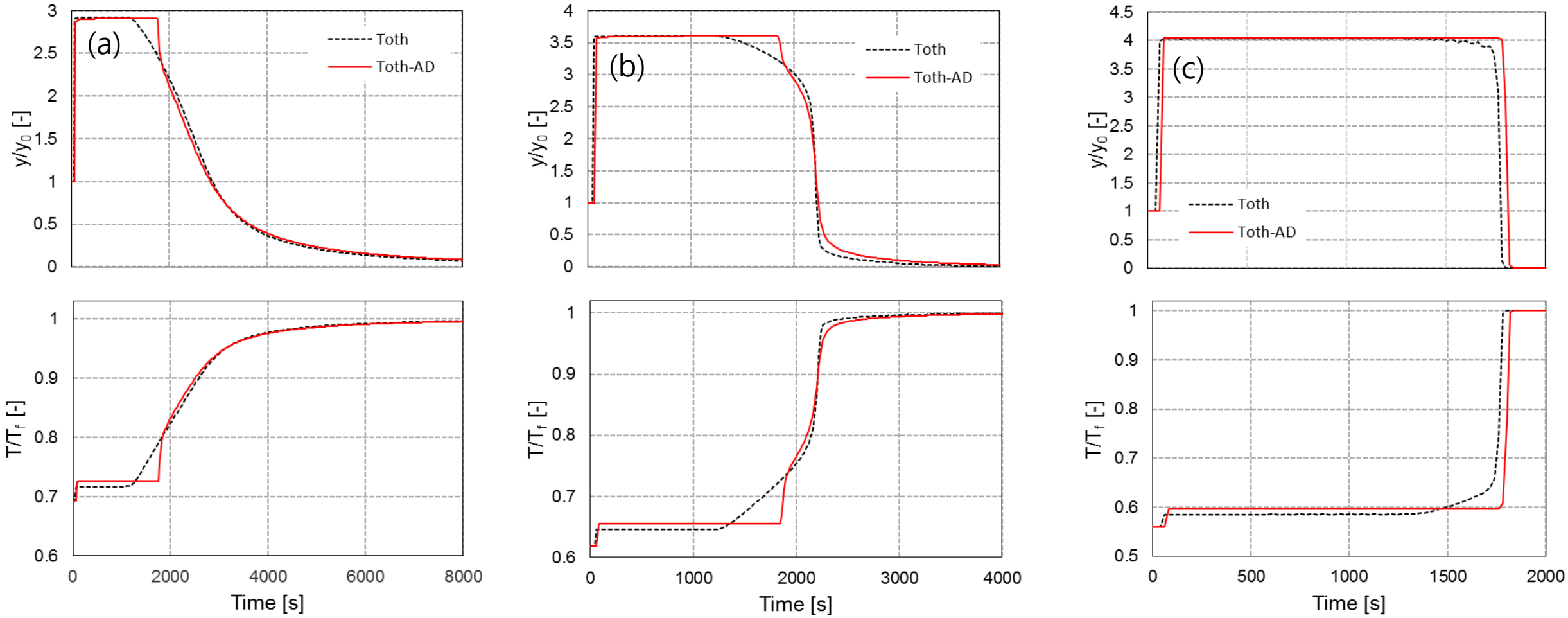


Figure 8. Thermal regeneration profiles with Toth and Aranovich-Donohue model with Toth by Equilibrium Theory at (a) 423K, (b) 473K and (c) 523K.

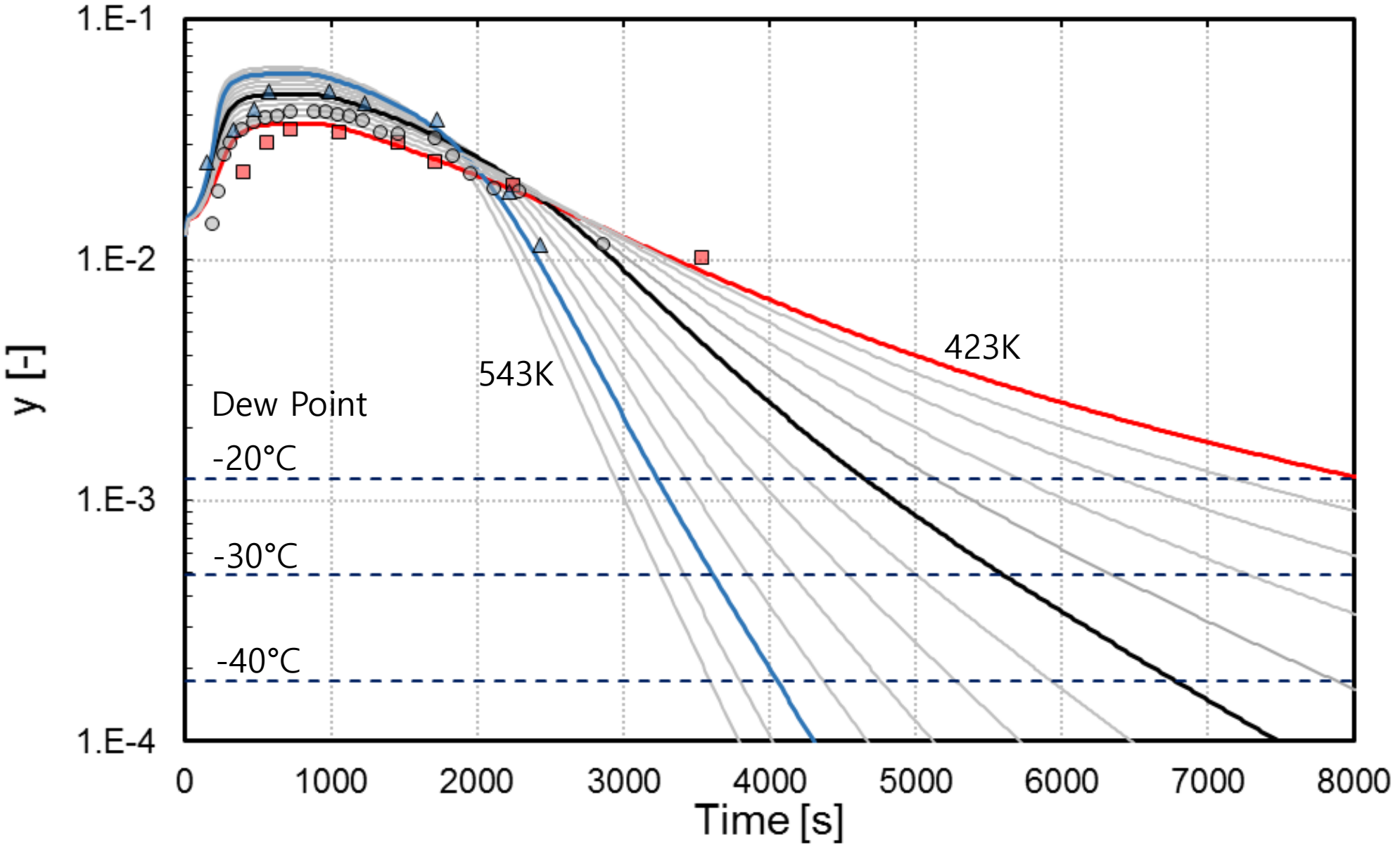


Figure 9. Full numerical simulation of thermal regeneration by hot nitrogen (symbols: experiment, lines: numerical simulation) in the range of 423 to 543K in the interval of 10K.

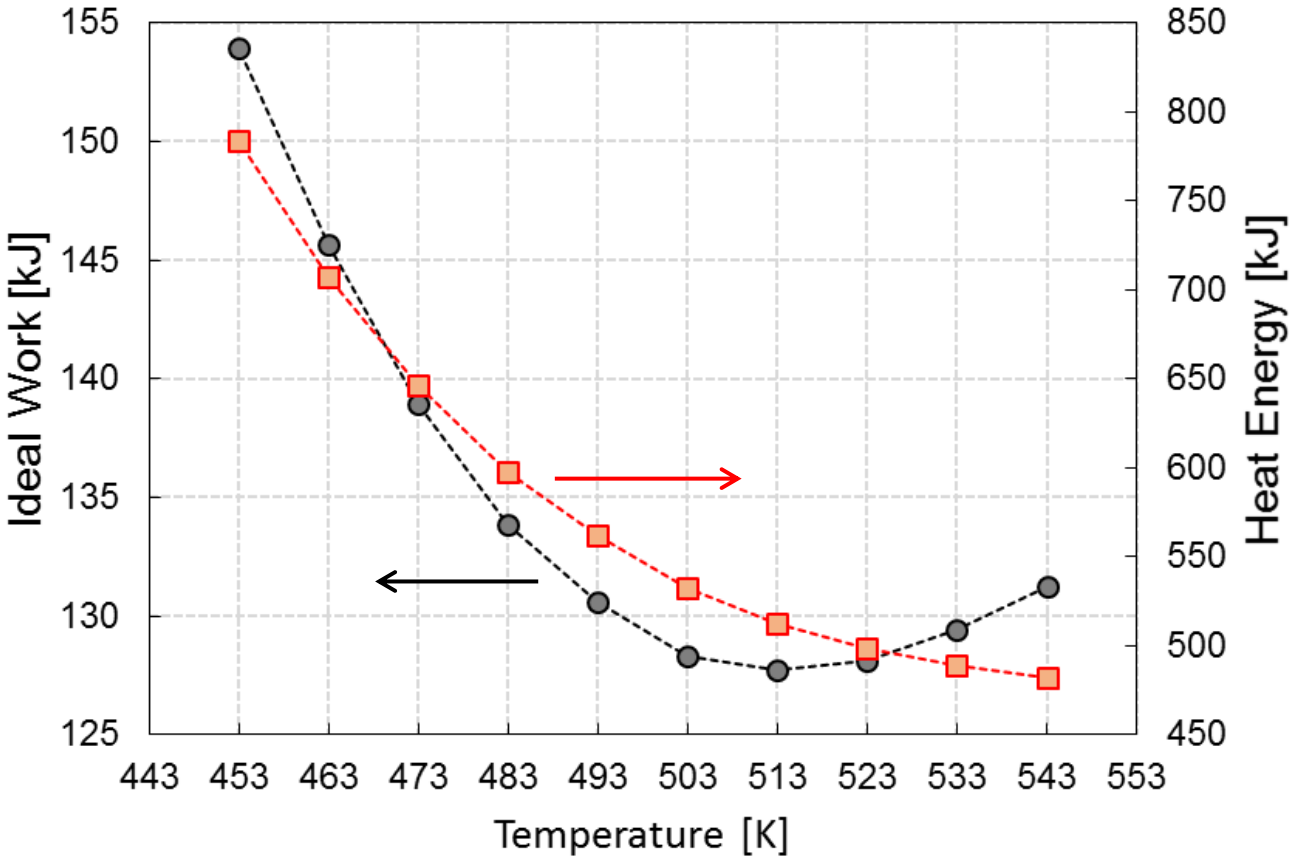


Figure 10. Change of total Ideal work and energy consumption with purge gas temperature in thermal regeneration up to –40 °C of dew point.